PROTEIN DESIGN

Design of stimulus-responsive two-state hinge proteins

Florian Praetorius[1,2]*†, Philip J. Y. Leung[1,2,3]†, Maxx H. Tessmer[4], Adam Broerman[1,2,5], Cullen Demakis[1,2,6], Acacia F. Dishman[1,2,7,8], Arvind Pillai[1,2], Abbas Idris[1,2,9], David Juergens[1,2,3], Justas Dauparas[1,2], Xinting Li[1,2], Paul M. Levine[1,2], Mila Lamb[1,2], Ryanne K. Ballard[1,2], Stacey R. Gerben[1,2], Hannah Nguyen[1,2], Alex Kang[1,2], Banumathi Sankaran[10], Asim K. Bera[1,2], Brian F. Volkman[7], Jeff Nivala[11,12], Stefan Stoll[4], David Baker[1,2,13]*

In nature, proteins that switch between two conformations in response to environmental stimuli structurally transduce biochemical information in a manner analogous to how transistors control information flow in computing devices. Designing proteins with two distinct but fully structured conformations is a challenge for protein design as it requires sculpting an energy landscape with two distinct minima. Here we describe the design of "hinge" proteins that populate one designed state in the absence of ligand and a second designed state in the presence of ligand. X-ray crystallography, electron microscopy, double electron-electron resonance spectroscopy, and binding measurements demonstrate that despite the significant structural differences the two states are designed with atomic level accuracy and that the conformational and binding equilibria are closely coupled.

Although many naturally occurring proteins adopt single folded states, conformational changes between distinct protein states are crucial to the functions of enzymes (*1*, *2*), cell receptors (*3*), and molecular motors (*4*). The extent of these changes ranges from small rearrangements of secondary structure elements (*5*, *6*) to domain rearrangements (*7*) to fold-switching or metamorphic proteins (*8*) that adopt completely different structures. In many cases, these conformational changes are triggered by "input" stimuli such as binding of a target molecule, post translational modification, or change in pH. These changes in conformation can in turn result in "output" actions such as enzyme activation, target binding, or oligomerization (*9*); protein conformational changes can thus couple a specific input to a specific output. The generation of proteins that can switch between two quite different structural states is a difficult challenge for computational protein design, which usually aims to optimize a single, very stable conformation to be the global minimum of the folding energy landscape (*10*, *11*). Design of such proteins requires reframing the design paradigm towards optimizing for more than one minimum on the energy landscape while simultaneously avoiding undesired off-target minima (*12*). Previously, multistate design has been used to design proteins that undergo very subtle conformational changes (*13*, *14*), cyclic peptides that switch conformations based on the presence of metal ions (*15*), and closely related sequences that fold into substantially different conformations (*16*). Stimulus-responsive "LOCKR" (Latching, Orthogonal Cage/Key pRotein) proteins have been designed to undergo conformational changes upon binding to a target peptide or protein (*17*). The "closed" unbound state of these "switch" proteins is a well-defined and fully structured conformation, but the "open" bound state is a broad distribution of conformations. The LOCKR platform has been used to generate biosensors (*18*, *19*), but he lack of a defined second state makes it poorly suited for mechanical coupling in molecular machines or discrete state-based computing systems.

[1]Department of Biochemistry, University of Washington, Seattle, WA, USA. [2]Institute for Protein Design, University of Washington, Seattle, WA, USA. [3]Graduate Program in Molecular Engineering, University of Washington, Seattle, WA, USA. [4]Department of Chemistry, University of Washington, Seattle, WA, USA. [5]Department of Chemical Engineering, University of Washington, Seattle, WA, USA. [6]Graduate Program in Biological Physics, Structure, and Design, University of Washington, Seattle, WA, USA. [7]Department of Biochemistry, Medical College of Wisconsin, Milwaukee, WI, USA. [8]Medical Scientist Training Program, Medical College of Wisconsin, Milwaukee, WI, USA. [9]Department of Bioengineering, University of Washington, Seattle, WA, USA. [10]Molecular Biophysics and Integrated Bioimaging, Lawrence Berkeley National Laboratory, Berkeley, CA, USA. [11]Paul G. Allen School of Computer Science and Engineering, University of Washington, Seattle, WA, USA. [12]Molecular Engineering and Sciences Institute, University of Washington, Seattle, WA, USA. [13]Howard Hughes Medical Institute, University of Washington, Seattle, WA, USA.
*Corresponding author. Email: flop@uw.edu (F.P.); dabaker@uw.edu (D.B.)
†These authors contributed equally to this work

Hinge Design Method

We set out to design proteins that can switch between two well-defined and fully structured conformations. To facilitate experimental characterization of the conformational change and to ensure compatibility with downstream applications, we imposed several additional requirements. First, the conformational change between the two states should be large, with some inter-residue distances changing by tens of angstroms between the two states. Second, the conformational change should not require global unfolding, which can be very slow. Third, neither of the two states should have substantial exposed patches of hydrophobic residues, which can compromise solubility. Fourth, the conformational change should be readily coupled to a range of inputs and outputs. Given that proteins are stabilized by hydrophobic cores, collectively achieving all of these properties in one protein system is challenging: protein conformations that differ considerably typically will have different sets of buried hydrophobic residues and require substantial structural rearrangements for interconversion.

We reasoned that these goals could be collectively achieved with a hinge-like design in which two rigid domains move relative to each other while remaining individually folded. The hinge amplifies small local structural and chemical changes to achieve large global changes whereas the chemical environment for most residues remains similar throughout the conformational change, avoiding the need for global unfolding. Provided that the two states of the hinge bury similar sets of hydrophobic residues, the amount of exposed hydrophobic surface area can be kept low in both states. Designing one of the resulting conformations to bind to a target effector couples the conformational equilibrium with target binding (Fig. 1A). This design concept has precedent in nature; for example, bacterial two-component systems use binding proteins that undergo hinging between two discrete conformations in response to ligand binding (*20*).

To implement this two-state hinge design concept, we took advantage of designed helical repeat proteins (DHRs) (*21*) (Fig. 1, B and C, left) and DHR-based junction proteins (*22*). The backbone conformation of the DHR serves as the first conformational state of our hinge protein ("state X"). To generate a second conformation, a copy of the parent protein is rotated around a "pivot helix" (Fig. 1, B and C) and a new backbone conformation is then created by combining the first half of the original protein ("domain 1"), the second half of the copy ("domain 2"), and either the helix following the pivot helix from the original protein or the helix preceding the pivot helix from the rotated copy ("peptide"). Rosetta FastDesign with backbone movement (*23*, *24*) is used to redesign the interface between the three parts, and the two domains are connected into a single chain using fragment-based loop closure (*21*, *25*, *26*). Using a combination of Rosetta two-state design (see methods section for details) and proteinMPNN (*27*) with linked residue identities, a single amino acid sequence is generated that is compatible with the state X hinge as well as with the state Y hinge-peptide complex. AlphaFold2 (AF2) (*28*) with initial guess (*29*) is then used to predict the structure of the hinge with and without the effector peptide, allowing for the selection of designs that are predicted in the correct state X in absence of the peptide and in the correct state Y complex in presence of the peptide. To favor designs that are predominantly in the closed state in absence of the peptide (Fig. 1, A and D), designs are selected only if state X

has lower energy (computed using Rosetta) than state Y in absence of the peptide, and if the state Y complex has lower energy than state X plus spatially separated peptide. Designs are also filtered on standard interface design metrics for the bound conformation (see Methods for details on filtering) (*30*).

Hinges bind effector peptides with sub-nanomolar to low micromolar affinities

We used our hinge design approach to generate hinge-peptide pairs that span a wide structural space (Figs. 1D and 2A and figs. S1 and S2). We experimentally tested multiple rounds of designs, using both DHRs (*21*) and helical junctions (*22*) as input scaffolds, and improving individual steps of the design pipeline between iterations (see Supplementary Note 1 for details on screening and a discussion of success rates and failure modes). We selected hinge and GFP-fused peptide designs that were soluble and interacted with each other as judged by size exclusion chromatography (SEC, figs. S2 and S3) and performed further characterization by fluorescence polarization (FP). Hinge-peptide binding affinities obtained from FP titration experiments with constant peptide concentration and varying hinge concentrations ranged from 1 nM to the low μM range (Fig. 2B, fig. S4, and table S1). To circumvent the bottleneck of finding soluble peptide sequences (see Supplementary Note 1), we also sought to design hinges that bind to a given target peptide. Starting from design cs201, we used a modified version of our design pipeline to redesign the hinge to bind peptides cs074B or cs221B, respectively, which have similar hydrophobic fingerprints as the original target peptide cs201B. This one-sided, two-state design approach yielded hinge designs that bound strongly to their new target peptide with little or no off-target binding (fig. S5).

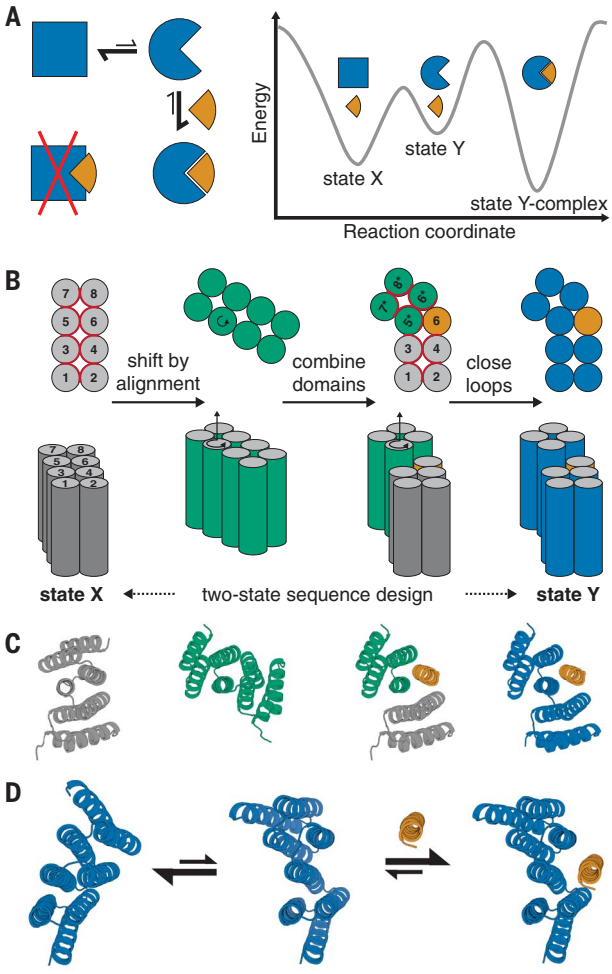

Fig. 1. Strategy for designing proteins that can switch between different conformations. (**A**) (Left) reaction scheme for a protein (blue) that undergoes a conformational change and can bind an effector (orange) in one (circle) but not in the other conformational state (square). (Right) Energy landscape for the system shown on the left. (**B**) Schematic representation of the hinge design approach. Alpha-helices are represented as circles (top view, top) or cylinders (side view, bottom). (From left to right) A previously designed repeat protein (gray) serves as the first conformation of the hinge. To generate the second conformation, a copy of the repeat protein (green) is moved by shifted alignment along a pivot helix, causing a rotation (top and bottom, indicated by the circular arrow) and a translation along the helix axis (bottom). The first 4 helices of the original protein form domain 1 of the hinge, the last 4 helices of the rotated copy form domain 2, and an additional helix is copied over from the original protein to serve as an effector peptide (orange) that can bind to this second conformation of the hinge. The two domains of the hinge are connected into one continuous chain (blue) using fragment-based loop closure, and a single amino acid sequence is designed to be compatible with both conformations. (**C**) Design steps from (B) illustrated using cartoon representations of an exemplary design trajectory. (**D**) Exemplary design models of a designed hinge protein in state X (left), state Y (center), and in state Y bound to an effector peptide (right). Hinge is shown in blue, peptide in orange.

Effector binding modulates the hinge conformational equilibrium

To characterize the conformational equilibrium of the designed hinges, we introduced two surface cysteine residues into the hinge protein and covalently labeled them with the nitroxide spin label MTSL (*31*). We then used double electron-electron resonance spectroscopy (DEER) to determine distance distributions between the two spin labels and compared these with simulated (*32*) distance distributions based on the state X and state Y design models. This experiment was performed on two different labeling site pairs for each design: one pair where the distance is predicted to decrease in the presence of peptide (Fig. 2C and S4, C and D) and the other where it is predicted to increase (Fig. 2D and fig. S4, C and D). In the absence of the peptide, the observed distance distributions closely matched the state X simulations. In all cases the distances between the two pairs of probes shifted upon addition of peptide to better match the state Y simulations, suggesting that addition of effector peptide causes the conformational equilibrium to shift toward state Y as designed. For example, cs074 (site pair 1) showed a clear peak between 40 and 50 Å in absence of the peptide, and a peak between 30 and 40 Å in presence of the peptide, and both peaks agree well with the corresponding simulations (Fig. 2C, top row). In a control experiment using the static parent DHR of design cs074, the distance distributions with and without peptide were identical and matched both the simulation for the parent design model, which closely resembles state X, and the experimental DEER distance distribution for state X of cs074 (fig. S4D).

We solved crystal structures for two designs, cs207 and cs074. For design cs207, crystals were obtained from two separate crystallization screens: one screen for the hinge alone, and one screen for the hinge in complex with the target peptide. In the absence of peptide the experimental structure agrees well with the state X design model (Fig. 3A), and the structure of the hinge-peptide complex agrees well with the state Y design model (Fig. 3B). The crystal structures of hinge cs207 in both designed states demonstrate the accuracy with which two very different conformational states of the same protein can now be designed. For design cs074, the crystal structure of the hinge-peptide complex agrees well with the corresponding state Y design model (Fig. 3C).

One major advantage of de novo designed proteins is their robustness to conditions that typically destabilize native proteins, such as high temperatures, and to structural perturbations, such as mutations, genetic fusion, and incorporation in designed protein assemblies. Circular dichroism (CD) melts show that the hinges remain folded at high temperatures (fig. S6), like the DHRs they were based on

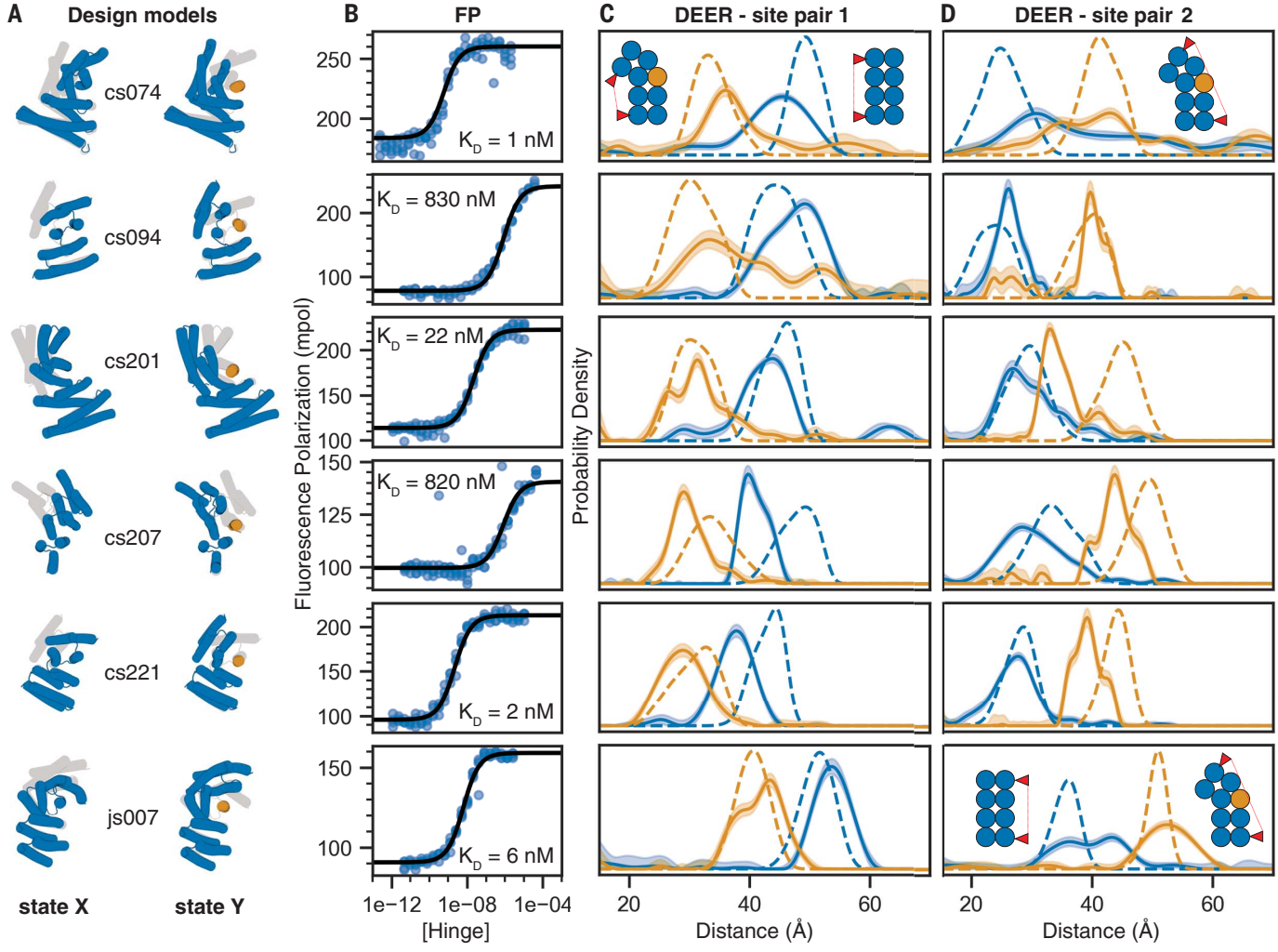

Fig. 2. Experimental validation of peptide-binding hinges. (**A**) Design models of hinges (blue) and peptides (orange) in state X (left model) and state Y bound to the peptide (right model). Gray shades behind models in state X and Y indicate the corresponding states Y and X, respectively. (**B**) Fluorescence polarization (FP) titrations with a constant concentration of TAMRA-labeled peptide (0.1 nM for cs074 and cs221; 0.5 nM for cs201; 1 nM for cs094, cs207, and js007) and varying hinge concentrations. Circles represent data points from four independent measurements; lines are fits of standard binding isotherms to all data points; and dissociation constants (K_D) are obtained from those fits. (**C** and **D**) Distance distributions between spin labels covalently attached to cysteine side chains. Solid lines are obtained from DEER experiments without (blue) or with (orange) an excess of peptide, shaded areas are 95% confidence intervals, and dashed lines are simulated based on the design models for state X (blue) or the state Y complex (orange). For each hinge two different label site pairs were tested, one in which the distance was expected to decrease with peptide binding (C) and one in which the distance was expected to increase upon peptide binding (D). Chemically synthesized peptides were used for all measurements except for cs074 site pair 1, for which sfGFP-peptide fusion was used. For design cs094, the residual state X peak in presence of the peptide likely reflects incomplete binding due to weak binding affinity or insufficient peptide concentration.

(*21*). To test whether our hinges can be incorporated as components of more complex protein assemblies without affecting their ability to undergo conformational changes, we designed a fully structured C3-symmetric protein with three hinge arms (Fig. 3D). We used inpainting (*33*) with RoseTTAFold (*34*) to rigidly connect one end of hinge cs221 to a previously validated homotrimer (*35*, *36*) and the other end of the hinge to a previously validated monomeric protein (*37*). Negative-stain electron microscopy (nsEM) with reference-free class averaging shows straight arms in absence of peptide and bent arms in presence of peptide cs221B, corroborating the designed conformational change (Fig. 3D and fig. S7).

A critical feature of two-state switches in biology and technology is the coupling between the state control mechanism and the populations of the two states. To quantitatively investigate the thermodynamics and kinetics of the effector-induced switching between the two states of our designed hinges, we used Förster resonance energy transfer (FRET). To increase both the absolute distance from N- to C- terminus and the change in termini distance between the two conformational states, we took advantage of the extensibility of repeat proteins and extended hinges cs201, cs221, and cs074 by 1 to 2 helices on their N and C termini, yielding cs201F, cs221F, and cs074F, respectively (Fig. 4A, first column). Single cysteines were introduced in helical regions near the termini of the extended hinges and stochastically labeled with an equal mixture of donor and acceptor dyes. For cs201F, the dye distance is above R_0 in state X and below R_0 in state Y, and hence acceptor emission upon donor excitation decreases upon addition of peptide cs201B (Fig. 4A, second column). For hinges cs074F and cs221F the distance between the label sites is above the R_0 of the dye pair in state X and below R_0 in state

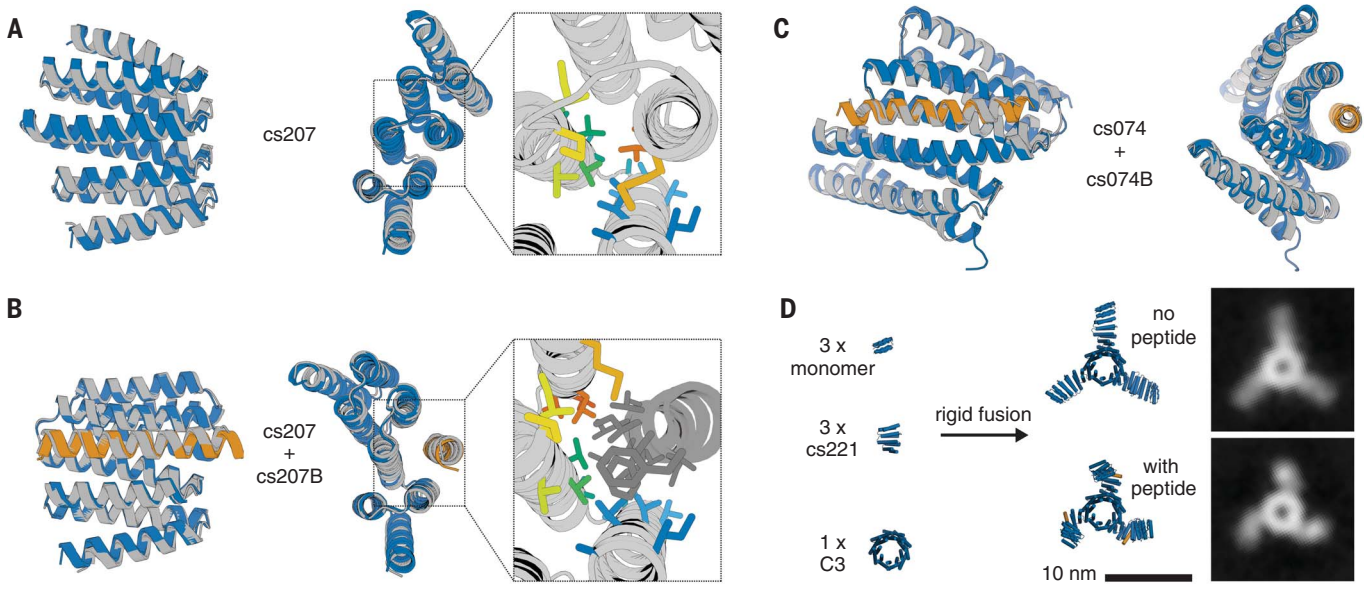

Fig. 3. Close agreement between crystal structures and design models for both designed states. (**A**) Design model (blue) of hinge cs207 in state X overlaid with crystal structure (gray) of hinge cs207 crystallized without peptide. Right panel shows a close-up view of the side chains in the interface between the two hinge domains (side chain colors follow a spectrum from blue to red from N- to C-terminus). (**B**) Design model (hinge in blue, peptide in orange) of the cs207 state Y hinge-peptide complex overlaid with crystal structure (gray) of hinge cs207 co-crystallized with peptide cs207B. Right panel shows a close-up view of the side chains in the interface between hinge and peptide [hinge side chain colors match the corresponding side chains in (A) and peptide side chains are shown in dark gray]. (**C**) Design model (hinge in blue, peptide in orange) of hinge cs074 in state Y overlaid with crystal structure (gray) of hinge cs074 co-crystallized with peptide cs207B. Representative electron densities for all crystal structures are shown in fig. S19. RMSD values between design model and experimental structure are given in table S4. (**D**) (Left) Components for design of a C3-symmetric homotrimer with three cs221 hinge arms. (Center) Design model of the hinge-armed trimer in state X (top) and in state Y (bottom). (Right) nsEM class averages of the trimer in absence (top) and in presence (bottom) of peptide cs221B.

Y and hence acceptor emission upon donor excitation increases upon addition of the corresponding peptides cs074B and cs221B, respectively (Fig. 4A, second column). We used labeled, extended DHR82, the parent protein for cs074F, as a static control, and observed fluorescence spectra comparable to cs074F but observed no change in fluorescence upon addition of the peptide (fig. S8, A and B). To test specificity of our hinge-peptide pairs, we performed pairwise titrations of all three labeled hinges at 2 nM with all three target peptides at varying concentrations. The on-target titrations had sigmoidal transitions that can be fitted with standard binding isotherms (Fig. 4A, third column; S8C), whereas the off-target titrations for cs201F and cs221F show flat lines, indicating no conformational change of these hinges upon addition of off-target peptides at micromolar concentrations. cs074F showed weak off-target binding that was three orders of magnitude weaker for cs201B and two orders of magnitude weaker for cs221B compared with the on-target interaction for cs074B. cs201F and cs221F are thus orthogonal from the nanomolar to the micromolar range, and the set of cs201F, cs221F, and cs074F is orthogonal over two orders of magnitude of effector concentration.

Association kinetics for the on-target interactions measured using constant concentrations of labeled hinge and varying excess concentrations of peptide are well fit by single exponentials (Fig. 4A, fourth column, and fig. S9). The apparent rate constants increase linearly with increasing peptide concentration, exhibiting standard pseudo–first order kinetics for bimolecular reactions (Fig. 4A, fifth column, and fig. S9). We analyzed these data using a model comprising three states (X, Y, Y+peptide) and four rate constants (Fig. 4B). The kinetic measurements using the FRET system follow the decrease in state X over time (d[X]/dt) upon the addition of peptide. The observed pseudo–first order behavior (Fig. 4A, fifth column) indicates that the conformational change happens on a timescale that is faster than that of the observed binding and can be treated as a fast pre-equilibrium (Supplementary Note 2). The slopes of the linear pseudo-first order fits (k_{on}) can thus be interpreted as the product of the microscopic association rate k_2 and the fractional population of state Y in absence of the peptide (F_Y = [Y]/([X]+[Y]), see Supplementary Note 2). FP-based titrations and kinetic characterization using the unlabeled extended hinge cs074F in excess over the TAMRA(Tetramethylrhodamine)-labeled peptide cs074B agree well with the corresponding FRET experiments, further supporting the pre-equilibrium model (Fig. 4C and fig. S9). FP kinetics experiments for other hinge designs also follow pseudo-first order behavior with k_{on} values ranging from 2.5×10^3 $M^{-1}s^{-1}$ to 7.8×10^4 $M^{-1}s^{-1}$ (figs. S4B and S10). To study the reversibility of hinge conformational changes, we started with 30 nM of FRET-labeled hinge cs201F, added 200 nM peptide to drive the conformational change, and then added excess unlabeled hinge cs201 to compete away the peptide (Fig. 4D). The FRET signal decreased upon addition of the peptide, consistent with conformational change from state X to state Y, and then returned to nearly the original level upon addition of unlabeled hinge, indicating that the hinge conformational change is fully reversible.

To explore whether peptide-responsive hinges could be turned into protein-responsive hinges, we used inpainting with RoseTTAFold to add two additional helices to a validated effector peptide, resulting in fully structured 3-helix bundles (3hb). For nine of our validated hinges we designed and experimentally characterized these effector proteins using SEC (Fig 4E and figs. S11A and S12). Hinge-3hb binding was tested qualitatively by SEC and, for hinges which had a corresponding FRET construct, quantitatively with the FRET-labeled variant, and DEER was used in addition to FRET to confirm that 3hb binding caused the same conformational change as effector peptide binding (Fig. 4E,

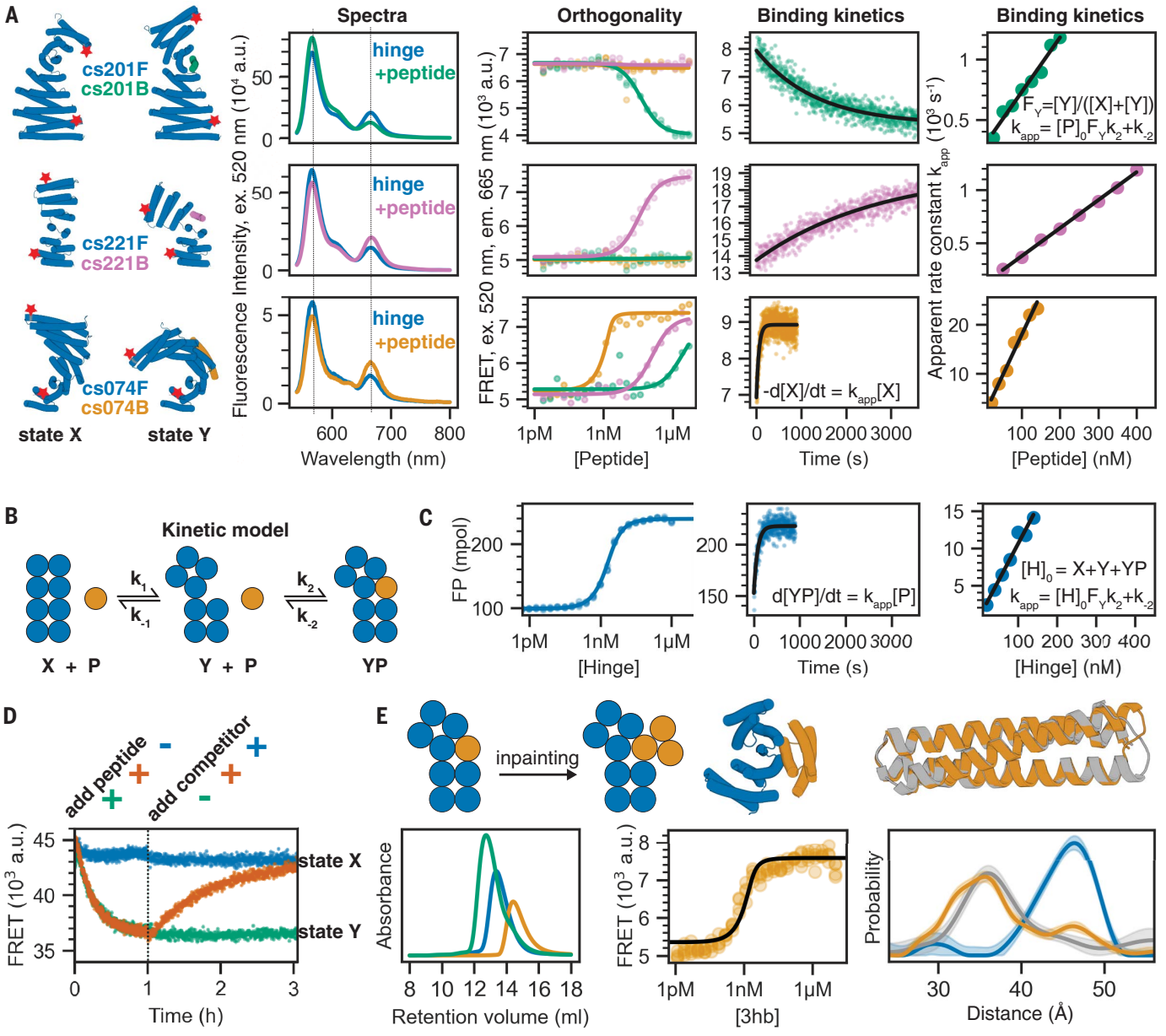

Fig. 4. Quantitative analysis of conformational changes in designed hinge proteins. (**A**) FRET-based characterization of three extended hinges. (From left to right) cylindrical representation of extended hinges (blue) and their corresponding target peptides (green, cs201B; pink, cs221B; orange, cs074B) with red stars indicating attachment sites for fluorescent dyes; fluorescence spectra (excitation at 520 nm) of labeled hinge without (blue) or with (green/pink/orange) target peptide; FRET-based binding titrations (excitation 520 nm, emission 665 nm) at 2 nM labeled hinge and varying peptide concentrations fitted with standard binding isotherms (solid lines); time course after mixing 2 nM (cs201F, cs074F) or 5 nM (cs221F) labeled hinge and 100 nM peptide fitted with a single-exponential equation (black line); and apparent rate constants obtained from single-exponential kinetic fits plotted against absolute peptide concentrations (circles) and fitted with a linear equation (black line). Dotted lines in spectra indicate acceptor and donor emission peaks. (**B**) Kinetic model describing the coupling of the conformational equilibrium to the binding equilibrium. X and Y, hinge in state X and Y, respectively; P, peptide; YP, peptide bound to hinge in state Y. k_1, k_{-1}, k_2, and k_{-2} are the microscopic rate constants. (**C**) FP characterization of unlabeled extended hinge cs074F. (From left to right) binding titration at 0.1 nM TAMRA-labeled peptide and varying hinge concentrations; time course after mixing 2 nM TAMRA-labeled peptide and 100 nM hinge fitted with a single-exponential equation (black line); apparent rate constants obtained from single-exponential kinetic fits plotted against absolute hinge concentrations (circles) and fitted with a linear equation (black line). (**D**) FRET-based reversibility experiment using the labeled extended hinge cs201F introduced in (C). Hinge concentration is 30 nM for all traces; 1 μM peptide is added at t = 0 (green/orange), 3 μM unlabeled competitor hinge is added after 1 h (blue/orange). (**E**) (Top from left to right) schematic representation of the inpainting procedure that adds two helices to the peptide cs074B yielding a three-helix bundle (3hb); cylindrical representation of 3hb_05 (orange) bound to hinge cs074 (blue); overlay of design model (orange) and crystal structure (gray) of 3hb_05. (Bottom from left to right) SEC traces for hinge cs074 (blue), 3hb_05 (orange), and a mixture of both (green); FRET-based titration of 2 nM extended labeled hinge cs074F and varying concentrations of 3hb_05 fitted with a standard binding isotherm (back line); Distance distributions obtained from DEER experiments as described in Fig. 2 (blue, cs074; gray, cs074 + peptide cs074B; orange, cs074 + 3hb_05).

bottom, and fig. S11). The affinity of 3hb05 to cs074F was similar to the affinity observed for the original peptide cs074B (Fig. 4E), whereas 3hb21 bound its target hinge cs221F significantly tighter than the original peptide cs221B (fig. S13). The 3hb approach was able to rescue designs for which the peptide alone or the hinge-peptide complex had shown the tendency to form higher-order oligomers (fig. S12). For two designs, 3hb05 and 3hb12, we obtained crystal structures that agreed well with the design models, indicating that the three-helix bundles are fully structured in isolation (Fig. 4E, top right, and fig. S14).

The conformational pre-equilibrium controls effector binding

To test the effect of the conformational pre-equilibrium on effector binding, we introduced disulfide "staples" that lock the hinge in one conformation. Using FP we analyzed peptide binding to stapled versions of hinge cs221 (Fig. 5, A and B). The variant that forms a disulfide bond in state X ("locked X") showed only weak residual binding, likely due to a small fraction of hinges not forming the disulfide (Fig. 5A). Upon addition of the reducing agent dithiothreitol (DTT) to break the disulfide, peptide binding was fully restored, making this hinge variant a red/ox–dependent peptide binder that binds the effector peptide under reducing—but not oxidizing—conditions. The association rate for the locked Y variant was 200 times higher than that for the original hinge without disulfides (Fig. 5B and fig. S15, A and B; despite this increase the overall binding affinity was weaker, suggesting the disulfide may lock the hinge in a slightly perturbed version of state Y). Using the pre-equilibrium model described above, the observed association rates provide an estimate of the fraction of hinge that is in state Y in absence of the peptide: a 200-fold higher observed on rate for the locked Y variant indicates a 200-fold higher fraction of hinge in state Y compared with the original hinge. Assuming that the locked Y variant is 100% in state Y and assuming that the microscopic rate constant k_2 is identical for the locked Y hinge and state Y of the original hinge, this would indicate that the original hinge is 99.5% in state X and 0.5% in state Y at equilibrium.

Having established the edge cases of locked state X and locked state Y, we sought to tune the pre-equilibrium by introducing single point mutations expected to specifically stabilize one state over the other while not directly affecting the peptide-binding interface. We used proteinMPNN to generate consensus sequences (*38*) for each state and identified non-interface positions with distinct residue preferences that were different between both states (Fig. 5C and fig. S16A). We experimentally tested individual protein variants carrying substitutions expected to stabilize one state over the other without disrupting either conformation, as evaluated by AF2 predictions. Consistent with coupling of the conformational and binding equilibria, substitutions based on state X consensus sequences led to weaker peptide binding, and those based on state Y consensus sequences led to stronger binding (Fig. 5C and fig. S15C). The substitutions that stabilized state Y showed accelerated association kinetics (Fig. 5C and fig. S17), consistent with our kinetic model (Fig. 4B and fig. S16, B and C; Supplementary Note 2): the mutations effectively shift

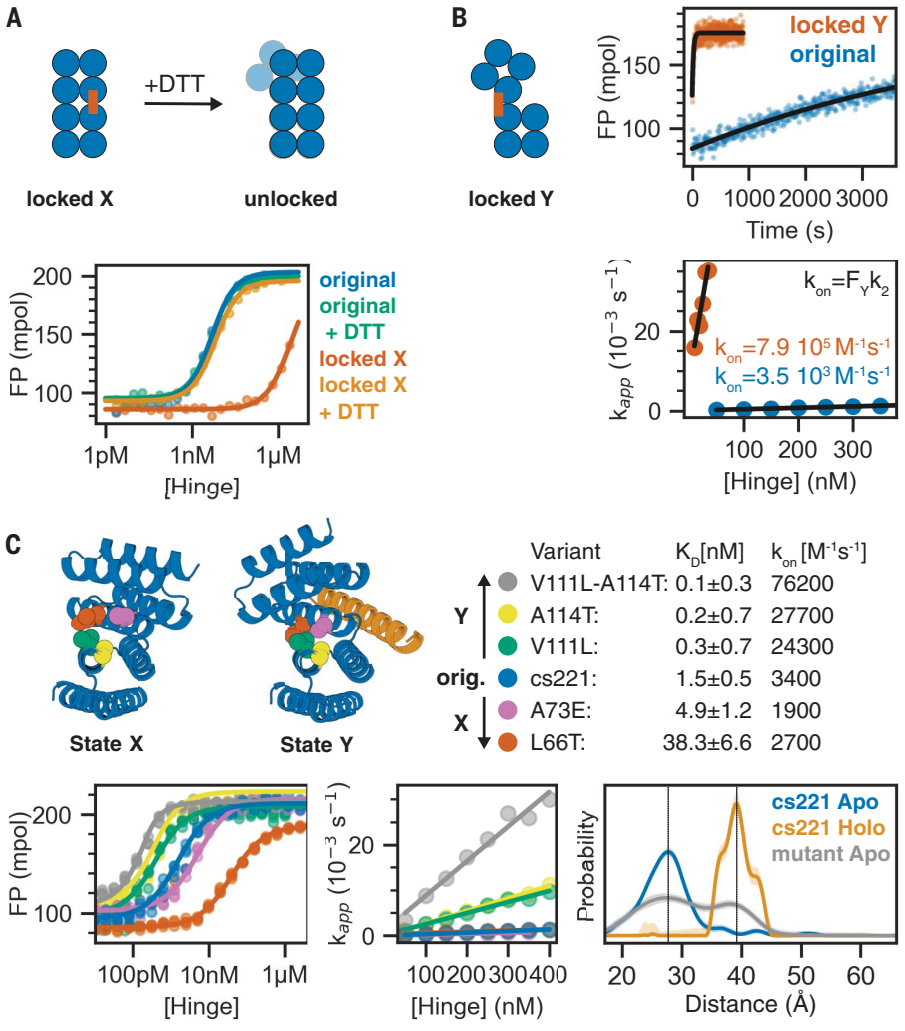

Fig. 5. Controlling the conformational pre-equilibrium affects peptide binding. (**A**) (Left) Schematic representation of a hinge containing two cysteine residues that can form a disulfide bond in state X but not in state Y, effectively locking the hinge in state X under oxidizing conditions. Upon addition of reducing agent DTT the disulfide bond is broken and the conformational equilibrium is restored. (Right) FP-based titration of 1 nM TAMRA-labeled peptide and a hinge with state X disulfide (red, orange) or the parent hinge without cysteines (blue, green) under oxidizing (blue, red) or reducing (green, orange) conditions. (**B**) (Top left) schematic representation of a hinge that is disulfide-locked in state Y; (Top right) time course after mixing 2 nM TAMRA-labeled peptide and 50 nM locked hinge (red) or original hinge without cysteines (blue) fitted with a single-exponential equation (black line); (Bottom) apparent rate constants obtained from single-exponential kinetic fits plotted against absolute hinge concentrations (circles) and fitted with a linear equation (black line). (**C**) Tuning the pre-equilibrium with point mutations. (Top left) Models of hinge cs221 in both states highlighting positions of point mutations. (Top right) Dissociation constants (K_D) and observed binding rate constants (k_{on}). (Bottom left) FP-based titration of 0.1 nM (yellow, green, blue) or 1 nM (pink, red) TAMRA-labeled peptide cs221B and varying concentrations of hinge variants containing one or two point mutations. (Bottom center) Apparent rate constants obtained from single-exponential kinetic fits plotted against absolute hinge concentrations (circles) and fitted with a linear equation (black line). (Bottom right) DEER distance distribution for the double mutant cs221-V111L-A114T in absence of peptide (gray) in comparison to the original cs221 with (orange) and without (blue) peptide. Vertical lines serve as a guide to the eye indicating state X and state Y distances.

the conformational pre-equilibrium toward state Y, increasing the on rates. This close coupling of the conformational equilibrium with association kinetics further supports the model outlined in Fig. 4B, and the fine tunability should be useful in downstream applications.

The state Y–stabilizing double mutant cs221_V111L_A114T has an on rate that is 22 times higher than that of the original cs221, suggesting that the occupancy of state Y in cs221_V111L_A114T is 22 times higher in the absence of peptide. Distance distributions obtained from DEER measurements on site pair 2 of the double mutant cs221_V111L_A114T in absence of the peptide indeed showed an additional peak at a distance closely matching state Y (Fig. 5C and fig. S18). DEER measurements on site pair 1 of the double mutant showed a broader distribution with occupancy in the region corresponding to state Y (Fig. 5C and fig. S18). Measurements in the presence of the peptide were virtually indistinguishable from the original cs221 (fig. S18). The double mutant thus populates two distinct states in the absence of the effector, and collapses to one state upon effector addition (Fig. 5E and fig. S18). The observation of a significant state Y population at equilibrium in the absence of the peptide as predicted based on the kinetic measurements further corroborates that the mutations affect the conformational pre-equilibrium and provides strong support for our quantitative two-state model of the kinetics and thermodynamics of the designed hinge-effector systems.

Conclusion

Our hinge design method generates proteins that populate two well-defined and structured conformational states rather than adopting a heterogeneous mixture of structures and should be broadly applicable to design of functional proteins. Like transistors in electronic circuits, we can couple the switches to external outputs and inputs to create sensing devices and incorporate them into larger protein systems to address a wide range of outstanding design challenges. Hinges containing a disulfide that locks them in state X couple the input "red/ox state" to the output "target binding," where the target can be a peptide or a protein, and our FRET-labeled hinges couple the input "target binding" to the output "FRET signal." Our approach can be readily extended such that state switching is driven by naturally occurring rather than designed peptides: recently designed extended peptide binding proteins (*39*) resemble the state X of our hinges, and recent designs that bind glucagon, secretin, or neuropeptide Y (*40*) resemble the state Y of our hinges. Hinges based on such designs could thus provide new routes to applications in sensing and detection.

Stimulus-responsive protein assemblies that switch between two well-defined shapes or oligomeric states in the presence of an effector can now be built by incorporating the hinges as modular building blocks, which was not possible with the previous LOCKR switches as one of the LOCKR states is disordered. Installing enzymatic sites in hinges such that substrate binding favors one state and product release favors the other state should enable fuel-driven conformational cycling, a crucial step toward the de novo design of molecular motors. More generally, the ability to design two-state systems, and the designed two-state switches presented here, should enable protein design to go beyond static structures to more complex multistate assemblies and machines.

REFERENCES AND NOTES

1. J. B. Stiller *et al*., *Nature* **603**, 528–535 (2022).
2. S. J. Kerns *et al*., *Nat. Struct. Mol. Biol.* **22**, 124–131 (2015).
3. A. Bisello *et al*., *J. Biol. Chem.* **277**, 38524–38530 (2002).
4. T. Movassagh, K. H. Bui, H. Sakakibara, K. Oiwa, T. Ishikawa, *Nat. Struct. Mol. Biol.* **17**, 761–767 (2010).
5. W. A. Catterall, G. Wisedchaisri, N. Zheng, *Nat. Chem. Biol.* **16**, 1314–1320 (2020).
6. E. G. B. Evans, J. L. W. Morgan, F. DiMaio, W. N. Zagotta, S. Stoll, *Proc. Natl. Acad. Sci. U.S.A.* **117**, 10839–10847 (2020).
7. B. Arragain *et al*., *Nat. Commun.* **11**, 3590 (2020).
8. A. K. Kim, L. L. Porter, *Structure* **29**, 6–14 (2021).
9. J.-H. Ha, S. N. Loh, *Chemistry* **18**, 7984–7999 (2012).
10. P.-S. Huang *et al*., *Science* **346**, 481–485 (2014).
11. R. Koga *et al*., *Proc. Natl. Acad. Sci. U.S.A.* **117**, 31149–31156 (2020).
12. A. F. Dishman, B. F. Volkman, *Curr. Opin. Struct. Biol.* **74**, 102380 (2022).
13. N. H. Joh *et al*., *Science* **346**, 1520–1524 (2014).
14. J. A. Davey, A. M. Damry, N. K. Goto, R. A. Chica, *Nat. Chem. Biol.* **13**, 1280–1285 (2017).
15. V. K. Mulligan *et al*., *Protein Sci.* **29**, 2433–2445 (2020).
16. K. Y. Wei *et al*., *Proc. Natl. Acad. Sci. U.S.A.* **117**, 7208–7215 (2020).
17. R. A. Langan *et al*., *Nature* **572**, 205–210 (2019).
18. A. Quijano-Rubio *et al*., *Nature* **591**, 482–487 (2021).
19. J. Z. Zhang *et al*., *Nat. Biotechnol.* **40**, 1336–1340 (2022).
20. M. Wang *et al*., *Proc. Natl. Acad. Sci. U.S.A.* **117**, 30433–30440 (2020).
21. T. J. Brunette *et al*., *Nature* **528**, 580–584 (2015).
22. T. J. Brunette *et al*., *Proc. Natl. Acad. Sci. U.S.A.* **117**, 8870–8875 (2020).
23. F. Khatib *et al*., *Proc. Natl. Acad. Sci. U.S.A.* **108**, 18949–18953 (2011).
24. M. D. Tyka *et al*., *J. Mol. Biol.* **405**, 607–618 (2011).
25. N. Koga *et al*., *Nature* **491**, 222–227 (2012).
26. Y.-R. Lin *et al*., *Proc. Natl. Acad. Sci. U.S.A.* **112**, E5478–E5485 (2015).
27. J. Dauparas *et al*., *Science* **378**, 49–56 (2022).
28. J. Jumper *et al*., *Nature* **596**, 583–589 (2021).
29. N. Bennett *et al*., Improving de novo Protein Binder Design with Deep Learning. bioRxiv 2022.06.15.495993 [Preprint] (2022).
30. L. Cao *et al*., *Nature* **605**, 551–560 (2022).
31. L J. Berliner, J. Grunwal, H. O. Hankovszky, K. Hideg, *Anal. Biochem.* **119**, 450–455 (1982).
32. M. H. Tessmer, S. Stoll, chiLife: An open-source Python package for in silico spin labeling and integrative protein modeling. bioRxiv 2022.12.23.521725 [Preprint] (2022).
33. J. Wang *et al*., *Science* **377**, 387–394 (2022).
34. M. Baek *et al*., *Science* **373**, 871–876 (2021).
35. J. P. Hallinan *et al*., *Commun. Biol.* **4**, 1240 (2021).
36. R. D. Kibler *et al*., Stepwise design of pseudosymmetric protein hetero-oligomers. bioRxiv 2023.04.07.535760 [Preprint] (2023).
37. D. D. Sahtoe *et al*., *Science* **375**, eabj7662 (2022).
38. G. E. Crooks, G. Hon, J.-M. Chandonia, S. E. Brenner, *Genome Res.* **14**, 1188–1190 (2004).
39. K. Wu *et al*., *Nature* **616**, 581–589 (2023).
40. S. V. Torres *et al*., De novo design of high-affinity protein binders to bioactive helical peptides. bioRxiv 2022.12.10.519862 (2022).

ACKNOWLEDGMENTS

We thank B. I. M. Wicky, L. F. Milles, and D. D. Sahtoe for helpful discussions and technical support, A. Courbet for inspiring discussions, A. Philomin and A. Borst for EM support, and K. VanWormer and L. Goldschmidt for technical support. We thank the Advanced Light Source (ALS) beamline 8.2.2/8.2.1 at Lawrence Berkeley National Laboratory for x-ray crystallography data collection. The Berkeley Center for Structural Biology is supported in part by the National Institutes of Health (NIH), National Institute of General Medical Sciences, and the Howard Hughes Medical Institute. The ALS is supported by the Director, Office of Science, Office of Basic Energy Sciences and US Department of Energy (DOE) (DE-AC02-05CH11231). **Author contributions:** F.P. developed the hinge design concept. F.P. and P.J.Y.L. developed the computational hinge design pipeline. F.P. and P.J.Y.L. designed, screened, and characterized most hinges with help from C.D. and A.P. M.H.T. designed, performed and analyzed DEER experiments. S.S. analyzed DEER data and supervised research. C.D. developed the one-sided two-state design protocol and designed and tested hinges with swapped targets. A.B. designed and characterized 3-helix bundles with support from D.C.J. A.I. designed and characterized the hinge-armed trimer with support from A.B. A.I. performed electron microscopy and image processing with support from A.P. J.D. provided conceptual support for two-state sequence design. X.L., P.M.L., M.L., and R.K.B. synthesized and purified peptides. X.L., M.L., and R.K.B. performed LC-MS validation of proteins and peptides. S.R.G. performed additional protein purification. H.N., A.K., B.S., and A.K.B. determined crystal structures. A.F.D. and B.V. contributed conceptual support. D.B. and J.N. supervised research. F.P., P.J.Y.L., and D.B. wrote the manuscript. M.H.T. contributed to the manuscript. All authors read and commented on the manuscript. **Funding:** This work was supported by a Human Frontier Science Program Long Term Fellowship [LT000880/2019 (to F.P.)], the Open Philanthropy Project Improving Protein Design Fund (to P.J.Y.L., C.W.D., H.N., and D.B.), an NSF Graduate Research Fellowship [DGE-2140004 (to P.J.Y.L.)], NERSC award BER-ERCAP0022018 (to P.J.Y.L and D.B.), the Audacious Project at the Institute for Protein Design (to A.B., A.P., A.I., M.L., R.K.B., S.R.G., A.K., and D.B.), a gift from Microsoft (to D.J., J.D., and D.B.), a grant from DARPA supporting the Harnessing Enzymatic Activity for Lifesaving Remedies (HEALR) program [HR001120S0052 contract HR0011-21-2-0012, (to X.L., A.K.B., and D.B.)], the Defense Threat Reduction Agency (DTRA) grant # HDTRA1-19-1-0003 (to P.M.L.), NSF Award #2006864 (to J.N.), and the Howard Hughes Medical Institute (to D.B.). DEER measurements were supported by R01 GM125753 (to S.S.). The spectrometer used was funded by NIH grant S10 OD021557 (to S.S.). **Competing interests:** A provisional patent application will be filed prior to publication, listing F.P., P.J.Y.L., M.H.T., A.B., C.D., A.F.D., A.P., A.I., B.V., S.S., and D.B. as inventors or contributors. B.F.V. has ownership interests in Protein Foundry, LLC and XLock Biosciences, Inc. **Data and materials availability:** All data are available in the main text or as supplementary materials. Design models are available in supplementary file S2 and through Zenodo (*41*). Design scripts are available in supplementary file S3 and through Zenodo (*41*). Raw DEER data are available through Zenodo (*41*). Crystallographic datasets have been deposited in the Protein Data Bank (PDB) (accession codes 8FIH, 8FVT, 8FIT, 8FIN, and 8FIQ).

SUPPLEMENTARY MATERIALS

science.org/doi/10.1126/science.adg7731
Materials and Methods
Figs. S1 to S22
Tables S1 to S4
Supplementary Notes 1 and 2
Data S1 to S3
References (*41*–*64*)
MDAR Reproducibility Checklist

Submitted 24 January 2023; accepted 11 July 2023
10.1126/science.adg7731